

Optimal Microswimming

Abdallah Daddi-Moussa-Ider,¹ Hartmut Löwen,^{1,*} and Benno Liebchen^{2,†}

¹*Institut für Theoretische Physik II: Weiche Materie,
Heinrich-Heine-Universität Düsseldorf, D-40225 Düsseldorf, Germany*

²*Institute of Condensed Matter Physics, Technische Universität Darmstadt, 64289 Darmstadt, Germany*

(Dated: August 26, 2020)

Contrasting the well explored problem on how to steer a macroscopic agent like an airplane or a moon lander to optimally reach a target, “optimal microswimming”, i.e. the quest for the optimal navigation strategy for microswimmers, remains unsolved. Here, we systematically explore this problem and show that the characteristic flow field of microswimmers crucially influences the required navigation strategy to reach a target fastest. The resulting optimal trajectories can have remarkable and non-intuitive shapes, which qualitatively differ from those of dry active particles or motile macroagents. Our results provide generic insights into the role of hydrodynamics and fluctuations on optimal navigation at the microscale and suggest that microorganisms might have survival advantages when strategically controlling their distance to remote walls. In particular, when fluctuations are present, choosing the optimal strategy, which appropriately respects hydrodynamics, can halve the time to reach the target compared to cases microswimmers head straight towards it.

INTRODUCTION

The quest on how to navigate or steer to optimally reach a target is important e.g. for airplanes to save fuel while facing complex wind patterns on their way to a remote destination, or for the coordination of the motion of the parts of a space-agent to safely land on the moon. These classical problems are well-explored and are usually solved using optimal control theory [1]. Likewise, navigation and search strategies are frequently encountered in a plethora of biological systems, including the foraging of animals for food, [2] or of T cells searching for targets to mount an immune response [3]. Very recently there is a growing interest also in optimal navigation problems and search strategies [4–9] of microswimmers [10–12] and “dry” active Brownian particles [13–16]. These active agents can self-propel in a low-Reynolds-number solvent, and might play a key role in tomorrow’s nanomedicine as recently popularized e.g. in [17]. In particular, they might become useful for the targeted delivery of genes [18] or drugs [19, 20] and other cargo [21, 22] to a certain target (e.g. a cancer cell) through our blood vessels, requiring them to find a good, or ideally optimal, path towards the target avoiding e.g. obstacles and unfortunate flow field regions. In the following, we refer to the general problem regarding the optimal trajectory of a microswimmer towards a predefined target (point-to-point navigation) as “optimal microswimming”.

The characteristic differences between optimal microswimming and conventional optimal control problems for macroagents like airplanes, cruise-ships or moon-landers, root in the presence of a low-Reynolds-number solvent in the former problem only. They comprise (i) overdamped dynamics (ii) thermal fluctuations and (iii) long-ranged fluid-mediated hydrodynamic interactions with interfaces, walls and obstacles, all of which exclusively apply to microswimmers. Recent work has

unveiled the consequences (i) and partly of (ii) for the optimal navigation of dry active particles (and particles in external flow fields): Specifically, the very recent works [4, 5, 8, 9, 23–30] have pioneered the usage of reinforcement learning [31–33] e.g. to determine optimal steering strategies of active particles to optimally navigate towards a target position [4, 5, 8, 9] or to exploit external flow fields to avoid getting trapped in certain flow structures by learning smart gravitaxis [23]. Meanwhile, refs. [5, 6, 34] have used (deep) reinforcement learning to explore microswimmer navigation problems in mazes and obstacle arrays assuming global [5] or only local [6] knowledge of the environment. Very recent analytical approaches [7, 8] to optimal active particle navigation complement these works and allow testing machine-learned results [8, 9]. (In addition, note that a remarkable body of knowledge exists on the complementary problem of optimizing body-shape deformation of deformable swimmers with optimal control theory; see e.g. [35–37].) Despite this remarkable progress in recent years, (iii), and its interplay with (ii), remains an important open problem to understand optimal microswimming.

To fill this gap, in the present work, we systematically explore optimal microswimming in the presence of walls or obstacles, where hydrodynamic microswimmer-wall interactions are well known to occur [38–46], but whose impact on optimal microswimming is essentially unknown. Combining an analytical approach involving Pontryagin’s maximum principle [1, 47, 48] with numerical simulations, we find that in the presence of remote obstacles or walls, the shortest path is not fastest for microswimmers, even in the complete absence of external force or flow fields. Thus, unlike dry active particles (or light rays following Fermat’s principle), in the presence of remote obstacles microswimmers generically have to take excursions to reach their target fastest. To appreciate the consequences of this finding, consider a microswimmer

which can freely control its swimming direction (but not its speed) and aims to reach a predefined target in the presence of two obstacles (Fig. 1): While in the absence of hydrodynamics (dry active particle), the shortest path is optimal (blue), an actual microswimmer would take a qualitatively different path to reach its target fastest (red and green curves). More generally, note that the role of hydrodynamics on optimal microswimmer routes can be subtle and lead to counterintuitive trajectory-shapes: for example, while for force-dipole swimmers the sign of the coefficient is unimportant for optimal navigation and only the strength of the hydrodynamic interactions matter, for source-dipole swimmers the coefficient plays a decisive role for the resulting trajectory-shapes.

Remarkably, when fluctuations are present, the choice of the navigation strategy is particularly important for the resulting travelling time: in some parameter regimes we find that optimal microswimming halves the travelling time to reach a target compared to cases where the microswimmer heads straight towards it. Here, it turns out that optimal microswimming exploits hydrodynamics to effectively protect active particles from fluctuations. This offers a novel perspective on the motion of microorganisms near surfaces or interfaces: it suggests that microorganisms might have a survival advantage when actively regulating their distance to remote walls in order to approach a food source via a strategic detour, rather than greedily heading towards it in the first place. Besides these possible biological implications, our findings should serve as a generically important ingredient for future works on optimal navigation of active particles, because the latter are naturally subject to fluctuations and hydrodynamic interactions with walls and obstacles, which to date have been neglected in most optimal navigation problems.

RESULTS

Optimal microswimming: Let us first consider an active particle which moves according to $\dot{\mathbf{r}}(t) = (v_x(\mathbf{r}, t) \cos \psi(t), v_z(\mathbf{r}, t) \sin \psi(t)) + \sqrt{2D}\boldsymbol{\eta}(t)$ where $v_x(\mathbf{r}, t), v_z(\mathbf{r}, t)$ are the speed components of the swimmer and $\psi(t)$ determines the swimming direction. Here, D is the diffusion coefficient which determines the strength of thermal fluctuations; for now, we choose $D = 0$ but discuss fluctuations later. Given a predefined initial $\mathbf{r}(t = 0) = \mathbf{r}_A$ and terminal point $\mathbf{r}(T) = \mathbf{r}_B$ in the xz -plane, we ask for the optimal connecting trajectory minimizing the travel time T , when the swimmer is allowed to steer freely. (This may represent e.g. biological swimmers which steer through body shape deformations or synthetic swimmers controlled by external feedback). That is, $\psi(t)$ can be freely chosen, whereas $v_x(\mathbf{r}, t), v_z(\mathbf{r}, t)$ are controlled by the environment. This is a well-defined optimal control problem determining the opti-

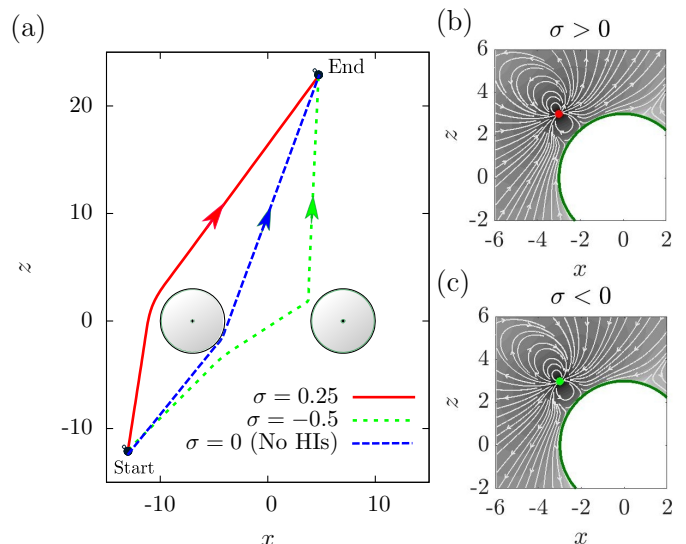


FIG. 1. (a) Optimal microswimming versus conventional optimal navigation in the presence of obstacles (gray disks): Curves show optimal trajectories for microswimmers (red and green) and for a dry active particle (blue). σ is the dimensionless source dipole strength and x, z are dimensionless coordinates. Panels (b),(c) show the flow field streamlines induced by a source dipole at the dimensionless position $\mathbf{r} = (-3, 3)$ in the presence of a spherical obstacle with dimensionless radius $R = 3$.

mal trajectory, the navigation protocol $\{\psi(t)|t \in [0, T]\}$ and T . It resembles classical navigation problems e.g. of an airplane, which can steer freely and moves at a speed which is determined by the wind (assuming some favorable constant engine power). Interestingly, however, while for such macroagents or dry active particles in constant external fields the shortest path is optimal [7, 49], for microswimmers excursions can pay off, as we will see in the following.

To develop an elementary understanding of optimal microswimming, let us first consider a source dipole microswimmer aiming to reach a target in the presence of a distant hard wall (far field), infinitely extended in the plane $z = 0$ (Fig. 2). Choosing length and time units as $x_u = L$ and $t_u = L/v_0$, with L, v_0 being the characteristic length of the swimmer and its bulk swimming speed, respectively, we have [50] $\dot{x} = f_x \cos \psi$, $\dot{z} = f_z \sin \psi$. Here dots represent time derivatives and $f_x = 1 - \sigma/(4z^3)$, $f_z = 1 - \sigma/z^3$; σ is the dimensionless source dipolar coefficient which is related to the physical source dipole coefficient via $\sigma_{\text{ph}} = L^3 v_0 \sigma$. For microswimmers achieving self propulsion through surface activity (ciliated microorganisms like Paramecium, active colloidal particles with uniform surface mobility) one expects $\sigma > 0$, whereas $\sigma < 0$ applies to some non-ciliated microswimmers with flagella [51]. To solve the optimal navigation problem, we first eliminate ψ from the equations of motion and then write the travel time

as $T = \int_{x_A}^{x_B} |\dot{x}|^{-1} dx = \int_{x_A}^{x_B} \mathcal{L}_{SD}(x, z(x), z'(x)) dx$, where the Lagrangian reads (see Methods for details):

$$\mathcal{L}_{SD} = |\dot{x}|^{-1} = \left(1/f_x^2 + (z'/f_z)^2\right)^{1/2}. \quad (1)$$

Now minimizing T , by solving Euler-Lagrange equations for \mathcal{L}_{SD} using shooting methods, determines the optimal trajectory $z(x)$, connecting \mathbf{r}_A and \mathbf{r}_B .

Similarly, the translational swimming velocities due to force dipolar hydrodynamic interactions (*E. coli*, *Chlamydomonas*) with a planar hard wall reads [50, 52] $\dot{x} = \cos\psi + 3\alpha\sin(2\psi)/(8z^2)$ and $\dot{z} = \sin\psi + 3\alpha(1 - 3\cos(2\psi))/(16z^2)$ where α is the dimensionless force dipolar coefficient ($\alpha = \alpha_{ph}/(L^2v_0)$). After some algebra, the resulting Lagrangian follows as (SI)

$$\mathcal{L}_{FD} = \left| \frac{72\alpha z^2 z'}{r_{\pm}^2 - 16z^4 - 27\alpha^2} \right|, \quad (2)$$

where r_{\pm} are the roots of a lengthy quartic polynomial, the coefficients of which are explicitly known functions of α^2 , z and z' (see Methods). The optimal swimming trajectories then result from solving the Euler-Lagrange equations.

As shown in Fig. 2, in the presence of an infinitely extended and distant flat wall, we find that both source and force dipole swimmers (and also force-quadrupole swimmers; see Methods) generically feature parabolic trajectories. That is, the microswimmers do not follow the shortest path to the target. Instead the parabolic trajectories represent the optimal compromise between maximizing speed and minimizing distance. Panel (a) illustrates this by showing that source dipoles with $\sigma > 0$ (which slow down when approaching the wall) take a parabola bended away from the wall, whereas those with $\sigma < 0$ prefer reducing their distance to the wall which speeds them up. In contrast to source dipole swimmers, perhaps surprisingly, for force dipole swimmers the shape of the resulting parabola depends only on the force dipole strength but not on the sign of the flow field. This pusher-puller-identity is generic for planar and spherical obstacle arrays which can be directly seen from the Lagrangian where only $|\alpha|$ and α^2 show up (Eq. (2)). Force quadrupolar microswimmers describing small microswimmers with elongated flagella [51, 53]), can also be solved using the Lagrangian approach (SI); their parabolic trajectories bent towards or away from the wall depending on the sign of the force quadrupole coefficient.

Based on these results we can now understand why hydrodynamic interactions with obstacles can have a drastic impact on the required navigation strategy to cross an obstacle field fastest. As shown in Fig. 1 without hydrodynamic interactions the agent takes the shortest path (blue curve), whereas a (source dipole) microswimmer with $\sigma = 0.25$ tends to avoid the obstacle and is faster

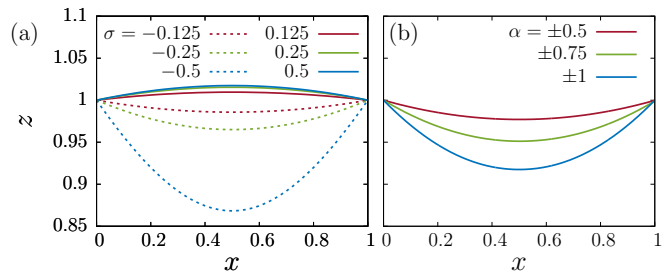


FIG. 2. Optimal microswimmer trajectories minimizing travel times between $\mathbf{r}_A = (0, 1)$ and $\mathbf{r}_B = (1, 1)$ for source dipole swimmers (a) and force dipole swimmers (b) in the presence of a hard and infinitely extended wall in the plane $z = 0$.

when taking the (longer) red path. For $\sigma = -0.5$ the microswimmer speeds up near the obstacles and chooses yet another and significantly longer path involving a close encounter with both obstacles. This shows that optimal microswimming requires a navigation strategy which qualitatively differs from the optimal strategy for dry active particles or macroagents.

Navigation in a fluctuating environment: In the world of microswimmers, fluctuations often play an important role. Besides Brownian noise which significantly displaces small biological microorganisms or active colloids on their way to a target, steering errors (or delay effects [54]) can effectively lead to fluctuations even in larger microswimmers. We now set $D \neq 0$, assuming that D does not significantly depend on space for simplicity. (Note that accounting for rotational diffusion e.g. to represent imperfect steering, does not qualitatively change the following results.) Let us now compare the following two different navigation strategies: The first one, which we call the “straight swimming strategy” is to steer straight towards the target at each instant of time. An alternative strategy is to re-calculate the optimal path of the underlying noise-free problem at each point in time, using the present position as a starting point, and to steer in the correspondingly determined direction. We refer to this as the “optimal swimming strategy”. While the latter strategy is of course expected to be better at weak noise, for strong noise, one might expect the opposite. However, in our simulations we find that the optimal swimming strategy notably outperforms the straight swimming strategy over the entire considered noise regime (Fig. 3 a), i.e. from $d = 0$ up to $d := D/(Lv_0) \approx 0.7$ (which is close to the maximum noise strength for which the swimmer reaches the target at all in our simulations). Interestingly, the difference between the two strategies increases with the noise strength (Fig. 3 a), such that the choice of the swimming strategy gets more and more important for a microswimmer as fluctuations become important. This finding might be

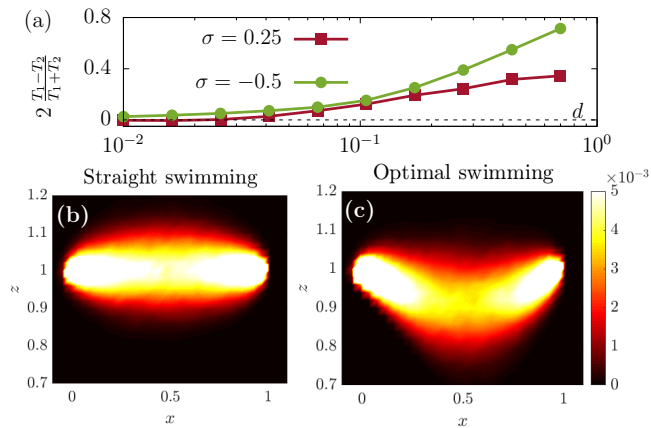


FIG. 3. Competition of navigation strategies in a fluctuating environment: (a) Relative travel-time difference between the straight swimming strategy (travel time T_1) and the optimal swimming strategy (T_2) for source dipole swimmers as a function of $d = D/(Lv_0)$. (b,c) Probability distribution (averaged over 5000 trajectories) of the coarse-grained position of a microswimmer navigating from $\mathbf{r}_A = (0, 1)$ to $\mathbf{r}_B = (1, 1)$ for $\sigma = -0.5$ and $d = 10^{-2}$. The target counts as reached when the microswimmer enters a domain of dimensionless size $\Delta x \times \Delta z = 0.04 \times 0.02$ around \mathbf{r}_B .

relevant e.g. for small microswimmers (with $\sigma < 0$) when trying to reach a food source: they do much better when seeking the proximity of nearby walls first, rather than greedily heading straight towards the target.

To understand these observations, consider the case $\sigma < 0$ where optimal swimming tends to reduce the microswimmer-wall distance and guides the swimmer to locations where hydrodynamic interactions are comparatively important and where the swimmer is fast (Fig. 3 b and Methods). Thus, for $\sigma < 0$ the swimmer can steadily approach the target for comparatively large d -values. In contrast, when following the straight swimming strategy, nothing stops fluctuations from transferring the swimmer to regions where it is slow (Fig. 3 c and Methods). The swimmer is then dominated by noise at comparatively low d -values and might reach the target only after following a long and winding path.

Let us now discuss the case $\sigma > 0$, where optimal swimming again significantly reduces traveling times over the whole range of explored d -values, although the above mechanism does not apply, because swimmers slow down when they are close to the wall. To see the strategic advantage of optimal swimming also here, note that when following the straight swimming strategy, fluctuations may accidentally displace the swimmer to locations close to the wall, where it is slow. In contrast, the optimal swimming strategy makes the swimmer stay away from the wall and prevents it from getting trapped in regions where it is slow and dominated by noise.

Time-dependent microswimmers: We finally

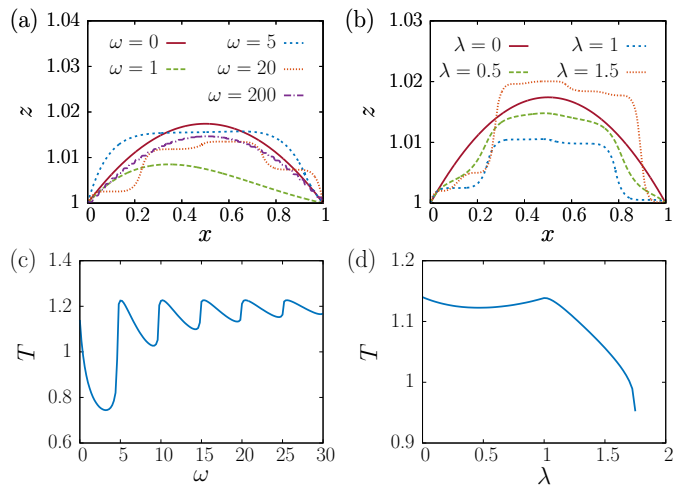


FIG. 4. Optimal trajectories and travel times of time-dependent source-dipole microswimmers for fixed amplitude $\lambda = 1$ and different dimensionless frequencies ω (a,c) and for fixed $\omega = \omega_{\text{ph}}L/v_0 = 6\pi$ and different λ (b,d). The shown travel times for the optimal trajectory are always shorter than when choosing the shortest path to the target. Driving law: $g_1(t) = 1 + \lambda \sin(\omega t)$ and $g_2(t) = g_1(t)^2$

complement our discussion of optimal microswimming by an exploration of time-dependent problems. This is inspired by microswimmers moving by body-shape deformations such as e.g. the algae *Chlamydomonas reinhardtii*, which alternately moves forward (stroke) and backwards (recovery stroke) and creates an oscillatory flow field [55]. We exemplarily consider a time-dependent source dipole swimmer with $f_x = g_1(t) - \sigma g_2(t)/(4z^3)$, $f_z = g_1(t) - \sigma g_2(t)/z^3$. (In physical units this corresponds to: $\dot{x} = [v_0 g_1(t) - \sigma_{\text{ph}} g_2(t)/(4z^3)] \cos \psi$, $\dot{z} = [v_0 g_1(t) - \sigma_{\text{ph}} g_2(t)/z^3] \sin \psi$.) While the case $g_1(t) = g_2(t)$ yields the same trajectories as in the time-independent case, for $g_1(t) \neq g_2(t)$ nontrivial trajectories occur (Fig. 4a,b). These trajectories can be determined exactly based on Pontryagin's maximum principle from optimal control theory [1, 47, 48] combined with a suitable transformation to treat the unknown terminal time as a dynamical variable (see Methods). Choosing e.g. $g_1(t) = 1 + \lambda \sin(\omega t)$ and $g_2(t) = g_1(t)^2$, yields optimal trajectories (Fig. 4a,b) which feature a characteristic step-plateau-like structure. Following such a trajectory the microswimmer mainly changes its distance from the wall in phases where it is slow, essentially to “improve” its distance from the wall for subsequent phases. When ω increases the plateau length decreases and for $\omega \rightarrow \infty$ the optimal trajectory approaches a parabola (purple curve in panel (a)) which differs from the optimal trajectory for $\lambda = 0$, because $\langle g_2(t) \rangle > 1$. The resulting travel time, monitored as a function of frequency (Fig. 4c), features a sequence of extrema occurring at frequencies where the swimmer reaches the target before completing a full driving cycle. For example, the global

minimum corresponds to $\omega = \omega_{\text{ph}}L/v_0 \approx \pi$ where the swimmer reaches the target at maximum speed without experiencing a phase where the swimmer is slower than its average speed ($\sin(\omega t) < 0$). The travel time also depends non-monotonously on λ ; it features a local minimum around $\lambda = 0.5$, where the time-average $\langle g_2(t) \rangle$ is smallest, and a local maximum at $\lambda = 1$. To understand the decrease of the travel time for $\lambda > 1$, note that for $\lambda > 1$ v temporarily changes sign. Since the swimmer can freely steer, $v < 0$ means that the swimmer immediately turns and swims forward again with an effective speed of $v_0|1 + \lambda \sin(\omega t)|$. This leads to an average swimmer speed which increases with λ , yielding the observed decrease of T . These exact results exemplify the complexity of time-dependent optimal microswimming and might serve as useful reference calculations to test machine-learning based approaches to optimal microswimming.

DISCUSSION

The message of this work is that optimal microswimming requires navigation strategies which qualitatively differ from those used to optimize the motion of dry active particles or motile macroagents like airplanes. This finding hinges on hydrodynamic interactions between microswimmers and remote boundaries, which obliges the swimmers to take significant detours to reach their target fastest, even in the absence of external fields. Such strategic detours are particularly useful in the presence of (strong) fluctuations: they effectively protect microswimmers against fluctuations and allow them to reach a food source or another target up to twice faster than when greedily heading straight towards it. This suggests that strategically controlling their distance to remote walls might benefit the survival of motile microorganisms – which serves as an alternative to the common viewpoint, that the microswimmer-wall distance is a direct (i.e. non-actively-regulated) consequence of hydrodynamic interactions.

Finally, our results might be relevant for future studies on microswimmers in various complex environments involving hard walls or obstacle landscapes [56–58], penetrable boundaries [59, 60] or external (viscosity) gradients [61–63]. For such scenarios our results (or generalizations based on the same framework) can be used as reference calculations e.g. to test machine learning based approaches to optimal microswimming [5, 6] and perhaps also to help programming navigation systems for future microswimmer generations.

METHODS

Here we discuss details regarding the two approaches used to solve optimal microswimming problems based on a La-

grangian approach and on Pontryagin’s maximum principle respectively. Both approaches lead to identical results but have been found to be advantageous in different situations: the Lagrangian approach leads to a boundary value problem which is more immediate to implement, numerically simpler and more robust than the corresponding higher-dimensional problem resulting from Pontryagin’s principle. The latter in turn allows for solving more general problems applying e.g. also to explicitly time-dependent microswimmers.

Lagrangian approach to optimal microswimming:

Following the Lagrangian optimization approach, a necessary condition for minimizing $T = \int_{x_A}^{x_B} |\dot{x}|^{-1} dx = \int_{x_A}^{x_B} \mathcal{L}(x, z(x), z'(x)) dx$ follows from the Euler-Lagrange equation

$$\frac{d}{dx} \frac{\partial \mathcal{L}}{\partial z'} - \frac{\partial \mathcal{L}}{\partial z} = 0. \quad (3)$$

First, considering source-dipolar hydrodynamic interactions with the interface, as given in the main body of the paper, we readily obtain upon simplification the following second-order differential equations

$$A(z)z''(x) + B(z)z'(x)^2 + C(z) = 0, \quad (4)$$

where we have defined the coefficients

$$A(z) = z(x) (z(x)^3 - \sigma) (4z(x)^3 - \sigma)^3, \quad (5a)$$

$$B(z) = -3\sigma (2z(x)^3 + \sigma) (4z(x)^3 - \sigma)^2, \quad (5b)$$

$$C(z) = 48\sigma (z(x)^3 - \sigma)^3. \quad (5c)$$

Equations (4) and (5) subject to Dirichlet boundary condition of imposed vertical distance at the start and end points can readily be solved numerically using a computer algebra software by means of a standard shooting method.

Next, for force-dipolar hydrodynamic interactions, we proceed as follows. By solving for the orientation angle ψ the dynamical equation providing the swimming velocity normal to the interface \dot{z} , four distinct solutions are obtained

$$\psi_{1,2} = \arctan(A_+, \pm B_+), \quad (6a)$$

$$\psi_{3,4} = \arctan(A_-, \pm B_-), \quad (6b)$$

where we have defined the arguments

$$A_{\pm} = \frac{1}{9\alpha} (-4z^2 \pm \phi_1), \quad (7a)$$

$$B_{\pm} = \frac{1}{9\alpha} (\phi_2 \pm 8z^2\phi_1)^{1/2}, \quad (7b)$$

where

$$\phi_1 = (72\alpha z^2 \dot{z} + 27\alpha^2 + 16z^4)^{1/2}, \quad (8a)$$

$$\phi_2 = 2(-36\alpha z^2 \dot{z} + 27\alpha^2 - 16z^4). \quad (8b)$$

Note that, for $a, b \in \mathbb{R}$, the function $\arctan(b, a)$ returns the principal value of the argument of the complex number $c = a + ib$. Specifically [64],

$$\arctan(b, a) = -i \ln \left(\frac{c}{|c|} \right) \in (-\pi, \pi], \quad (9)$$

where $|c| = (a^2 + b^2)^{1/2}$.

By inserting Eqs. (6) into the dynamical equation for the swimming velocity parallel to the interface \dot{x} , setting $\dot{z} = z'\dot{x}$, and solving the resulting equations for \dot{x} , we readily obtain

$$\dot{x} = \frac{1}{72\alpha z^2 z'} (r_{\pm}^2 - 16z^4 - 27\alpha^2), \quad (10)$$

where r_{\pm} are the roots of the quartic polynomial

$$P_{\pm}(Z) = a_0 \pm a_1 Z + a_2 Z^2 + \pm a_3 Z^3 + a_4 Z^4, \quad (11)$$

the coefficients of which are explicitly given by

$$a_0 = 9(16z^4 + 27\alpha^2)^2 + 256z'^2 z^4(16z^4 - 81\alpha^2),$$

$$a_1 = -64z'^2 z^2(16z^4 + 81\alpha^2),$$

$$a_2 = -6(3 + 2z'^2)(16z^4 + 27\alpha^2),$$

$$a_3 = 32z'^2 z^2,$$

$$a_4 = 9 + 4z'^2.$$

The nature of the roots of the quartic polynomial is primarily determined by the sign of the discriminant [65]. Assuming that z is a weakly-varying function about the value $h > 0$, such that $z(x) = h + \epsilon f(x)$, where $|\epsilon| \ll h$, the discriminants Δ_{\pm} of the polynomial function given by Eq. (11) can be expanded to leading order about $\epsilon = 0$ as

$$\Delta_{\pm} \sim K(27\alpha^2 + 16h^4)(3\alpha + 4h^2)(3\alpha - 4h^2)z'^4,$$

where K is a positive real number. In the far-field limit, we expect that $3\alpha \ll 4h^2$, and thus $\Delta_{\pm} < 0$. Accordingly, the polynomial functions has two distinct real roots and two complex conjugate non-real roots [66].

If we denote by r_1 and r_2 the real roots of P_+ then it can readily be noticed that $-r_1$ and $-r_2$ are the real roots of P_- since $P_-(-Z) = P_+(Z)$. Consequently, the system admits two possible Lagrangians, as can be inferred from Eq. (10).

The roots r_1 and r_2 can be obtained via computer algebra systems. They are not listed here due to their complexity and lengthiness.

Physically, the Lagrangian yielding the shortest traveling time is the one that needs to be considered [7].

Force-quadrupolar microswimmers: Finally, we investigate the optimal swimming due to force-quadrupolar hydrodynamic interactions with the interface. In this case, the translational swimming velocities read [50, 53]

$$\dot{x} = \cos \psi + \frac{\nu \cos \psi}{32z^3} (27 \cos(2\psi) - 13), \quad (13a)$$

$$\dot{z} = \sin \psi + \frac{\nu \sin \psi}{8z^3} (9 \cos(2\psi) + 5), \quad (13b)$$

where ν is the dimensionless force quadrupolar coefficient related to the force quadrupolar coefficient in physical units ν_{ph} via $\nu_{\text{ph}} = L^3 \nu_0 \nu$. Solving Eq. (13a) for ψ yields three possible distinct values

$$\psi_1 = \arccos(\phi_+), \quad (14a)$$

$$\psi_2 = \pi - \arccos\left(\frac{1}{2}\phi_+ - i\frac{\sqrt{3}}{2}\text{sign}(\nu)\phi_-\right), \quad (14b)$$

$$\psi_3 = \pi - \arccos\left(\frac{1}{2}\phi_+ + i\frac{\sqrt{3}}{2}\text{sign}(\nu)\phi_-\right), \quad (14c)$$

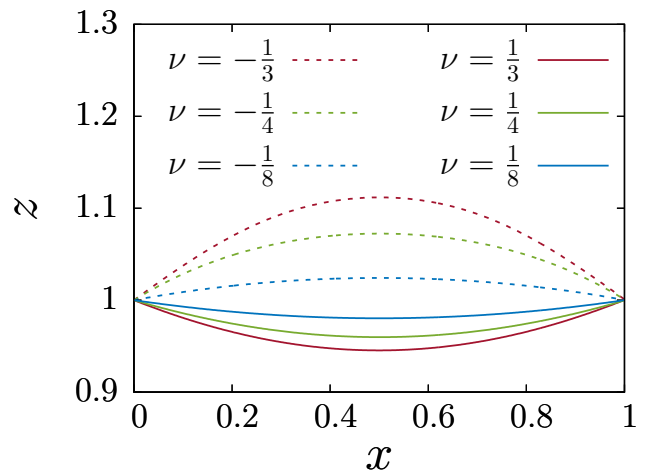


FIG. 5. Optimal microswimmer trajectories to get fastest from $\mathbf{r}_A = (0, 1)$ to $\mathbf{r}_B = (1, 1)$ for force quadrupole swimmers with dimensionless force quadrupole strength ν , in the presence of a hard wall infinitely extended in the plane $z = 0$.

where sign denotes the sign function, such that $\text{sign}(\nu) = \nu/|\nu|$. In addition, we have defined for convenience the abbreviations $Z = z^3/\nu$ and $C = \nu^3(27\dot{x}Z + f^{1/2})$. Moreover,

$$f = 64Z^3 + 3(243\dot{x}^2 - 80)Z^2 + 300Z - 125, \quad (15)$$

and

$$\phi_{\pm} = \frac{2}{9} \left(\frac{C^{1/3}}{\nu} \pm \frac{\nu(5 - 4Z)}{C^{1/3}} \right). \quad (16)$$

Substituting the expression of ψ_1 given by Eq. (14a) into Eq. (13b), using the fact that $\dot{z} = z'\dot{x}$, and solving the resulting equation for \dot{x} yields

$$\dot{x} = \frac{1}{54z^3} \left(\frac{\rho^3}{\nu^2} - \frac{\nu}{\rho^3} (4z^3 - 5\nu)^3 \right), \quad (17)$$

where ρ denotes the roots of explicitly-known polynomial of degree 12. In the physical range of parameters, this polynomial admits either one real radical having the order of multiplicity four or three distinct radicals also having the order of multiplicity four.

It turned out that the same set of radicals are obtained when making substitution with ψ_2 or ψ_3 .

In order to proceed further, we evaluate numerically the Lagrangians and accurately fit the results using a standard nonlinear bivariate hypothesis of the form

$$\mathcal{L}(z, z') = \sum_{m=0}^N \sum_{n=0}^N a_{ij} z^m z'^n, \quad (18)$$

where a_{ij} are fitting parameters. Here, we have taken $N = 4$ but checked that taking larger values does not alter our results.

In Fig. 5, we present exemplary optimal swimming trajectories for force quadrupole swimmers near a no-slip wall infinitely extended in the plane $z = 0$. As already mentioned in

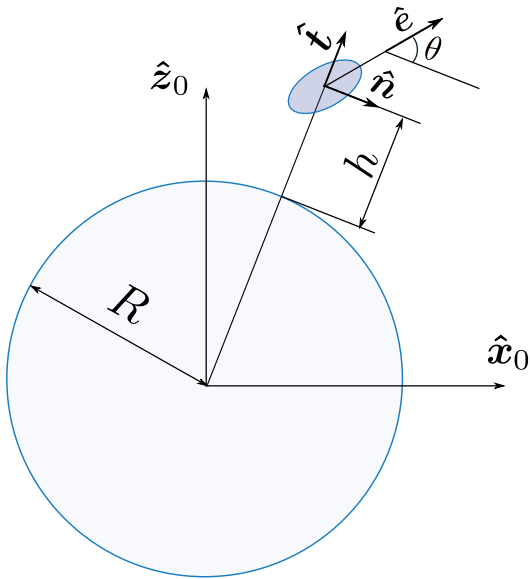


FIG. 6. Graphical illustration of a microswimmer moving near a spherical boundary.

the main body of the paper, the optimal swimming trajectory depend on the sign of the force quadrupolar coefficient where for $\nu > 0$ (resp. $\nu < 0$) the swimmer tend to swim toward (resp. away from) the interface before reaching the target.

***Hydrodynamic interactions near spherical boundaries:**

The translational swimming velocities resulting from source dipolar hydrodynamic interactions with a solid sphere of radius R positioned at the origin of coordinates (see Fig. 6) can be decomposed into two terms

$$\mathbf{V} = \hat{\mathbf{e}} + \mathbf{v}^{\text{HI}}, \quad (19)$$

with $\hat{\mathbf{e}} = \cos \theta \hat{\mathbf{n}} + \sin \theta \hat{\mathbf{t}}$ denoting the instantaneous orientation angle of the swimmer, and

$$\mathbf{v}^{\text{HI}} = P \sin \theta \hat{\mathbf{t}} + Q \cos \theta \hat{\mathbf{n}}, \quad (20)$$

quantifies the effect of hydrodynamic interactions with the spherical boundary. This contribution can readily be determined from the Green's function near a rigid sphere [67]. Here, we have defined for convenience

$$P = -\frac{\sigma R (3h^2 + 6hR + 8R^2)}{h^3 (h + 2R)^3}, \quad (21a)$$

$$Q = \frac{\sigma R (3h^2 + 6hR + 4R^2) (h^2 + 2hR - 2R^2)}{4h^3 (h + 2R)^3 (h + R)^2}, \quad (21b)$$

where, again, we have scaled lengths by a characteristic length scale of the swimmer L , and velocities by the bulk swimming speed v_0 .

Without loss of generality, we consider motion in the plane $y = 0$.

To obtain the translational swimming velocities near two obstacles, as illustrated in Fig. 1 a of the main text, we use the commonly-employed superposition approximation [68]. The

latter conjectures that that the solution for the Green's function near two widely-separated obstacles can conveniently be approximated by superimposing the contributions due to each obstacle independently. Accordingly,

$$\mathbf{V} = \hat{\mathbf{e}} + \mathbf{v}_1^{\text{HI}} + \mathbf{v}_2^{\text{HI}}, \quad (22)$$

where

$$\mathbf{v}_i^{\text{HI}} = P_i \sin \theta_i \hat{\mathbf{t}}_i + Q_i \cos \theta_i \hat{\mathbf{n}}_i, \quad i \in \{1, 2\}. \quad (23)$$

In addition,

$$\hat{\mathbf{e}} = \cos \theta_1 \hat{\mathbf{n}}_1 + \sin \theta_1 \hat{\mathbf{t}}_1 = \cos \theta_2 \hat{\mathbf{n}}_2 + \sin \theta_2 \hat{\mathbf{t}}_2. \quad (24)$$

By projecting Eqs. (22) through (24) along the unit vectors $\hat{\mathbf{t}}_i$ and $\hat{\mathbf{n}}_i$, eliminating the angles θ_1 and θ_2 , and solving the resulting equations for \dot{x} upon using the fact that $\dot{z} = z'\dot{x}$, the Lagrangian can readily be obtained explicitly. The Euler-Lagrange equation can then be solved numerically in Matlab using the `ode45` routine.

Optimal control theory for optimal microswimming: To solve the optimal navigation problem of time-dependent microswimmers we use Pontryagin's maximum principle [1, 47]. Thus, we first formulate a cost functional $P[\psi] = \int_0^T R(\mathbf{r}, \psi, t) dt$ where we choose $R = -1$ so that maximizing the cost corresponds to minimizing traveling time. We now introduce the optimal control Hamiltonian $H(\mathbf{r}, \mathbf{p}, t) = \mathbf{f} \cdot \mathbf{p} - 1$ where \mathbf{p} is the adjoint momentum and $\mathbf{f} = (f_x \cos \psi, f_y \sin \psi)$; where $f_x = 1 - \sigma/(4z^3)$ and $f_z = 1 - \sigma/z^3$ as discussed in the main text for source dipole swimmers. We now optimize H regarding the control variable ψ by solving $\partial_\psi H = 0$ with respect to ψ , yielding $\tan \psi^* = u_z/u_x$ where ψ^* is the optimal ψ and where we have defined $u_x = p_x(1 - \sigma/(4z^3))$ and $u_z = p_z(1 - \sigma/z^3)$. Now plugging ψ^* into H yields the optimal Hamiltonian which reads for source dipole swimmers $H^* = \pm \sqrt{u_x^2 + u_y^2} - 1$ (dimensional units). The optimal trajectory is now determined by the Hamilton equation $\dot{\mathbf{r}} = \partial_{\mathbf{p}} H^*$ and $\dot{\mathbf{p}} = -\partial_{\mathbf{x}} H^*$ which has to be solved as a boundary value problem, such that $\mathbf{r}(t=0) = \mathbf{r}_A$ and $\mathbf{r}(t=T) = \mathbf{r}_B$ where T is the unknown traveling time. That is, we have four first order differential equations and an unknown terminal time T , which together with the four boundary conditions and the fact that H is an integral of motion fully determines the solution. Note however that due to the unknown T the boundary value problem can not be straightforwardly solved by standard shooting approaches. Thus, we rescale time via $t = Tt'$ such that the terminal time is 1 in units of t' and treat $T =: a(t)$ as a dynamical variable which we determine along with $\mathbf{r}(t), \mathbf{p}(t)$ using multidimensional shooting. This approach is numerically somewhat more demanding and less robust compared to our Lagrangian approach but it is also more general and additionally allows solving problems for time-dependent swimmers e.g. for swimmers with dimensionless speed $g_1(t)$ (i.e. $v_{\text{ph}}(t) = v_0 g_1(t)$) and source dipole strength $\sigma g_2(t)$ ($\sigma_{\text{ph}}(t) = \sigma v_0 L^3 g_2(t)$) where $g_1(t), g_2(t)$ are time-dependent functions.

Distributions of microswimmer positions: Here we show additional figures visualizing the distribution of the positions of a source-dipole microswimmer on the way to its

target. These figures complement Fig. 3b,c of the main text and show corresponding results for $\sigma = -0.5$ (Fig. 7) and $\sigma = 0.25$ (Fig. 8), for different noise strengths d .

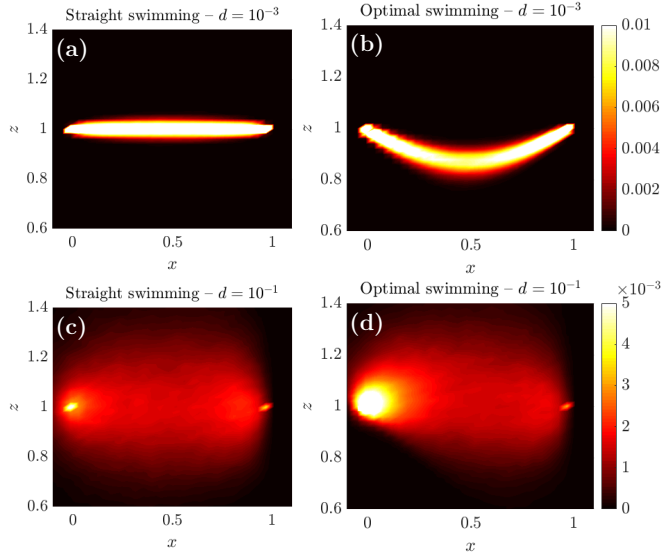


FIG. 7. Probability distribution of the position of a source-dipole microswimmer ($\sigma = -0.5$). d -values are shown in the key and details are as in Fig. 3b,c of the main text.

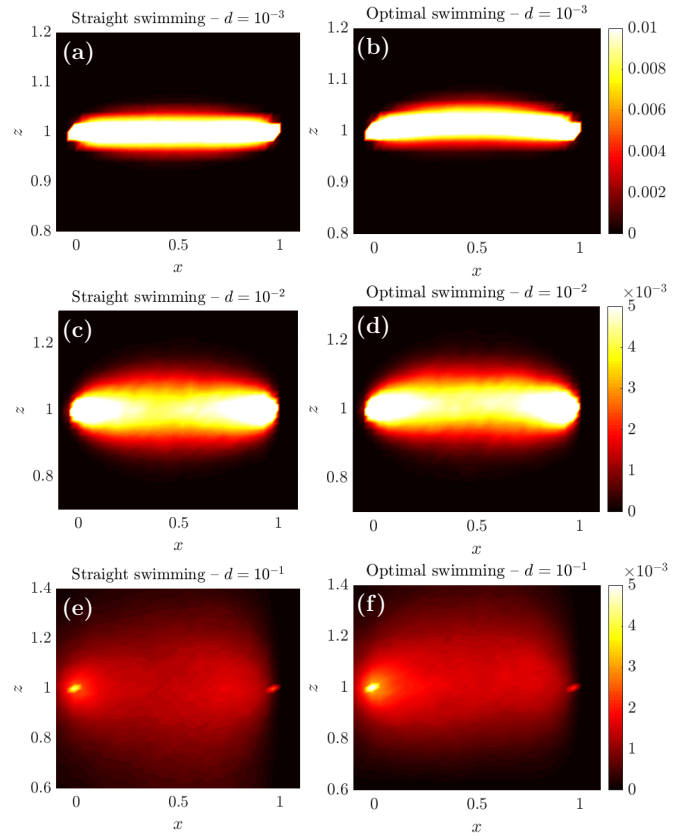


FIG. 8. As fig. 7 but for $\sigma = 0.25$.

ACKNOWLEDGMENTS

We thank A. M. Menzel for useful discussions and gratefully acknowledge support from the DFG (Deutsche Forschungsgemeinschaft) through projects DA 2107/1-1 and LO 418/23-1.

* hlowen@hhu.de

† liebchen@fkp.tu-darmstadt.de

- [1] Donald E Kirk, *Optimal control theory: an introduction* (Courier Corporation, 2004).
- [2] Gandhimohan M Viswanathan, Marcos GE Da Luz, Ernesto P Raposo, and H Eugene Stanley, *The Physics of Foraging: an Introduction to Random Searches and Biological Encounters* (Cambridge University Press, U.K., 2011).
- [3] G Matthew Fricke, Kenneth A Letendre, Melanie E Moses, and Judy L Cannon, “Persistence and adaptation in immunity: T cells balance the extent and thoroughness of search,” *PLoS Comput. Biol.* **12** (2016).
- [4] Santiago Muinos-Landin, Keyan Ghazi-Zahedi, and Frank Cichos, arXiv:1803.06425 (2018).
- [5] Yuguang Yang and Michael A Bevan, “Optimal navigation of self-propelled colloids,” *ACS Nano* **12**, 10712 (2018).
- [6] Yuguang Yang, Michael A Bevan, and Bo Li, “Efficient navigation of colloidal robots in an unknown environment via deep reinforcement learning,” *Adv. Intell. Sys.* **2**, 1900106 (2019).
- [7] Benno Liebchen and Hartmut Löwen, “Optimal navigation strategies for active particles,” *EPL* **127**, 34003 (2019).
- [8] Elias Schneider and Holger Stark, “Optimal steering of a smart active particle,” *EPL* **127**, 64003 (2019).
- [9] Luca Biferale, Fabio Bonaccorso, Michele Buzzicotti, Patricio Clark Di Leoni, and Kristian Gustavsson, “Zermelo’s problem: Optimal point-to-point navigation in 2D turbulent flows using reinforcement learning,” *Chaos* **29**, 103138 (2019).
- [10] Eric Lauga and Thomas R. Powers, “The hydrodynamics of swimming microorganisms,” *Rep. Prog. Phys.* **72**, 096601 (2009).
- [11] Jens Elgeti, Roland G Winkler, and Gerhard Gompper, “Physics of microswimmers – single particle motion and collective behavior: a review,” *Rep. Prog. Phys.* **78**, 056601 (2015).
- [12] Eric Lauga, “Bacterial hydrodynamics,” *Ann. Rev. Fluid Mech.* **48**, 105–130 (2016).
- [13] Pawel Romanczuk, Markus Bär, Werner Ebeling, Benjamin Lindner, and Lutz Schimansky-Geier, “Active Brownian particles,” *Eur. Phys. J. Spec. Top.* **202**, 1 (2012).
- [14] Clemens Bechinger, Roberto Di Leonardo, Hartmut Löwen, Charles Reichhardt, Giorgio Volpe, and Giovanni Volpe, “Active particles in complex and crowded environments,” *Rev. Mod. Phys.* **88**, 045006 (2016).
- [15] Andreas Zöttl and Holger Stark, “Emergent behavior in active colloids,” *J. Phys.: Condens. Matter* **28**, 253001 (2016).
- [16] Michael E Cates and Julien Tailleur, “Motility-induced phase separation,” *Annu. Rev. Condens. Matter Phys.* **6**, 219 (2015).
- [17] Yuval Noah Harari, *Homo Deus: A brief history of tomorrow* (Random House, 2016).
- [18] Famin Qiu, Satoshi Fujita, Rami Mhanna, Li Zhang, Benjamin R Simona, and Bradley J Nelson, “Magnetic helical microswimmers functionalized with lipoplexes for targeted gene delivery,” *Adv. Func. Mater.* **25**, 1666 (2015).
- [19] Byung-Wook Park, Jiang Zhuang, Oncay Yasa, and Metin Sitti, “Multifunctional bacteria-driven microswimmers for targeted active drug delivery,” *ACS Nano* **11**, 8910 (2017).
- [20] Joseph Wang and Wei Gao, “Nano/microscale motors: biomedical opportunities and challenges,” *ACS Nano* **6**, 5745 (2012).
- [21] Xing Ma, Kersten Hahn, and Samuel Sanchez, “Catalytic mesoporous Janus nanomotors for active cargo delivery,” *J. Am. Chem. Soc.* **137**, 4976 (2015).
- [22] Ahmet F Demirörs, Mehmet Tolga Akan, Erik Poloni, and André R Studart, “Active cargo transport with Janus colloidal shuttles using electric and magnetic fields,” *Soft Matter* **14**, 4741–4749 (2018).
- [23] Simona Colabrese, Kristian Gustavsson, Antonio Celani, and Luca Biferale, “Flow navigation by smart microswimmers via reinforcement learning,” *Phys. Rev. Lett.* **118**, 158004 (2017).
- [24] Kristian Gustavsson, Luca Biferale, Antonio Celani, and Simona Colabrese, *Eur. Phys. J. E* **40**, 110 (2017).
- [25] Simona Colabrese, Kristian Gustavsson, Antonio Celani, and Luca Biferale, *Phys. Rev. Fluids* **3**, 084301 (2018).
- [26] Byunghyun Yoo and Jinwhan Kim, “Path optimization for marine vehicles in ocean currents using reinforcement learning,” *J. Mar. Sci. Tech.* **21**, 334 (2016).
- [27] Gautam Reddy, Antonio Celani, Terrence J Sejnowski, and Massimo Vergassola, “Learning to soar in turbulent environments,” *Proc. Natl. Acad. Sci. U.S.A.* **113**, E487 (2016).
- [28] Gautam Reddy, Jerome Wong-Ng, Antonio Celani, Terrence J Sejnowski, and Massimo Vergassola, “Glider soaring via reinforcement learning in the field,” *Nature* **562**, 236 (2018).
- [29] Jaya Kumar Alageshan, Akhilesh Kumar Verma, Jérémie Bec, and Rahul Pandit, arXiv:1910.01728 (2019).
- [30] Alan Cheng Hou Tsang, Pun Wai Tong, Shreyes Nallan, and On Shun Pak, “Self-learning how to swim at low reynolds number,” *Physical Review Fluids* **5**, 074101 (2020).
- [31] Richard S Sutton, Andrew G Barto, *et al.*, *Introduction to reinforcement learning*, Vol. 135 (MIT press Cambridge, 1998).
- [32] Frank Cichos, Kristian Gustavsson, Bernhard Mehlig, and Giovanni Volpe, “Machine learning for active matter,” *Nat. Mach. Intell.* **2**, 94 (2020).
- [33] Paul Garnier, Jonathan Viquerat, Jean Rabault, Aurélien Larcher, Alexander Kuhnle, and Elie Hachem, “A review on deep reinforcement learning for fluid mechanics,” arXiv preprint arXiv:1908.04127 (2019).
- [34] Yuguang Yang, Michael A Bevan, and Bo Li, “Micro/nano motor navigation and localization via deep reinforcement learning,” arXiv preprint arXiv:2002.06775 (2020).
- [35] Laetitia Giraldi, Pierre Martinon, and Marta Zoppello, “Optimal design of purcell’s three-link swimmer,” *Phys. Rev. E* **91**, 023012 (2015).

- [36] François Alouges, Antonio DeSimone, and Aline Lefebvre, “Optimal strokes for low reynolds number swimmers: an example,” *J. Nonlinear Sci.* **18**, 277 (2008).
- [37] François Alouges, Antonio DeSimone, Laetitia Giraldo, Yizhar Or, and Oren Wiezel, “Energy-optimal strokes for multi-link microswimmers: Purcell’s loops and Taylor’s waves reconciled,” *New J. Phys.* **21**, 043050 (2019).
- [38] Jens Elgeti, U Benjamin Kaupp, and Gerhard Gompper, “Hydrodynamics of sperm cells near surfaces,” *Biophys. J.* **99**, 1018–1026 (2010).
- [39] Gao-Jin Li and Arezou M Ardekani, “Hydrodynamic interaction of microswimmers near a wall,” *Phys. Rev. E* **90**, 013010 (2014).
- [40] Jens Elgeti and Gerhard Gompper, “Wall accumulation of self-propelled spheres,” *Europhys. Lett.* **101**, 48003 (2013).
- [41] Ali Mozaffari, Nima Sharifi-Mood, Joel Koplik, and Charles Maldarelli, “Self-diffusiophoretic colloidal propulsion near a solid boundary,” *Phys. Fluids* **28**, 053107 (2016).
- [42] Yahaya Ibrahim and Tanniemola B Liverpool, “How walls affect the dynamics of self-phoretic microswimmers,” *Eur. Phys. J. Special Topics* **225**, 1843–1874 (2016).
- [43] Ali Mozaffari, Nima Sharifi-Mood, Joel Koplik, and Charles Maldarelli, “Self-propelled colloidal particle near a planar wall: A brownian dynamics study,” *Phys. Rev. Fluids* **3**, 014104 (2018).
- [44] Zaiyi Shen, Alois Würger, and Juho S Lintuvuori, “Hydrodynamic interaction of a self-propelling particle with a wall,” *Eur. Phys. J. E* **41**, 39 (2018).
- [45] Jens Elgeti and Gerhard Gompper, “Microswimmers near surfaces,” *Eur. Phys. J. Spec. Top.* **225**, 2333 (2016).
- [46] Matthias Laumann, Winfried Schmidt, Alexander Farutin, Diego Kienle, Stephan Förster, Chaouqi Misbah, and Walter Zimmermann, “Emerging attractor in wavy poiseuille flows triggers sorting of biological cells,” *Phys. Rev. Lett.* **122**, 128002 (2019).
- [47] Anthony T Fuller, “Bibliography of Pontryagm’s Maximum Principle,” *Int. J. Electron.* **15**, 513 (1963).
- [48] Ernest B Lee and Lawrence Markus, *Foundations of optimal control theory*, Tech. Rep. (Minnesota Univ Minneapolis Center For Control Sciences, U.S.A, 1967).
- [49] Max Born and Emil Wolf, “Principles of optics. 1999,” Press Syndicated, Cambridge: UK (1970).
- [50] Saverio E Spagnolie and Eric Lauga, “Hydrodynamics of self-propulsion near a boundary: predictions and accuracy of far-field approximations,” *J. Fluid Mech.* **700**, 105 (2012).
- [51] Arnold J. T. M. Mathijssen, Amin Doostmohammadi, Julia M. Yeomans, and Tyler N. Shendruk, “Hydrodynamics of microswimmers in films,” *J. Fluid Mech.* **806**, 35–70 (2016).
- [52] Allison P Berke, Linda Turner, Howard C Berg, and Eric Lauga, “Hydrodynamic attraction of swimming microorganisms by surfaces,” *Phys. Rev. Lett.* **101**, 038102 (2008).
- [53] Abdallah Daddi-Moussa-Ider, Maciej Lisicki, Christian Hoell, and Hartmut Löwen, “Swimming trajectories of a three-sphere microswimmer near a wall,” *J. Chem. Phys.* **148**, 134904 (2018).
- [54] Seyed Mohsen Jebreil Khadem and Sabine HL Klapp, “Delayed feedback control of active particles: a controlled journey towards the destination,” *Phys. Chem. Chem. Phys.* **21**, 13776 (2019).
- [55] Jeffrey S Guasto, Karl A Johnson, and Jerry P Gollub, “Oscillatory flows induced by microorganisms swimming in two dimensions,” *Phys. Rev. Lett.* **105**, 168102 (2010).
- [56] Giovanni Volpe, Ivo Buttinoni, Dominik Vogt, Hans-Jürgen Kümmerer, and Clemens Bechinger, “Microswimmers in patterned environments,” *Soft Matter* **7**, 8810 (2011).
- [57] Aidan T Brown, Ioana D Vladescu, Angela Dawson, Teun Vissers, Jana Schwarz-Linek, Juho S Lintuvuori, and Wilson CK Poon, “Swimming in a crystal,” *Soft Matter* **12**, 131 (2016).
- [58] Kilian Dietrich, Giovanni Volpe, Muhammad Nasruddin Sulaiman, Damian Renggli, Ivo Buttinoni, and Lucio Isa, “Active atoms and interstitials in two-dimensional colloidal crystals,” *Phys. Rev. Lett.* **120**, 268004 (2018).
- [59] Abdallah Daddi-Moussa-Ider, Segun Goh, Benno Liebchen, Christian Hoell, Arnold JTM Mathijssen, Francisca Guzmán-Lastra, Christian Scholz, Andreas M Menzel, and Hartmut Löwen, “Membrane penetration and trapping of an active particle,” *J. Chem. Phys.* **150**, 064906 (2019).
- [60] Abdallah Daddi-Moussa-Ider, Benno Liebchen, Andreas M Menzel, and Hartmut Löwen, “Theory of active particle penetration through a planar elastic membrane,” *New J. Phys.* **21**, 083014 (2019).
- [61] Benno Liebchen, Paul Monderkamp, Borge ten Hagen, and Hartmut Löwen, “Viscotaxis: Microswimmer navigation in viscosity gradients,” *Phys. Rev. Lett.* **120**, 208002 (2018).
- [62] Matthias Laumann and Walter Zimmermann, “Focusing and splitting streams of soft particles in microflows via viscosity gradients,” *Eur. Phys. J. E* **42**, 108 (2019).
- [63] Charu Datt and Gwynn J Elfring, “Active particles in viscosity gradients,” *Phys. Rev. Lett.* **123**, 158006 (2019).
- [64] Milton Abramowitz and Irene A Stegun, *Handbook of Mathematical Functions*, 5 (Dover New York, 1972).
- [65] A Akritas, *Elements of Computer Algebra with Applications* (John Wiley & Sons, Inc., Hoboken, New Jersey, U.S.A., 1989).
- [66] E. L. Rees, “Graphical discussion of the roots of a quartic equation,” *Amer. Math. Monthly* **29**, 51 (1922).
- [67] Saverio E Spagnolie, Gregorio R Moreno-Flores, Denis Bartolo, and Eric Lauga, “Geometric capture and escape of a microswimmer colliding with an obstacle,” *Soft Matter* **11**, 3396 (2015).
- [68] Eric R Dufresne, David Altman, and David G Grier, “Brownian dynamics of a sphere between parallel walls,” *EPL* , 264 (2001).